Atmospheric
Chemistry
and Physics
Discussions

SCIAMACHY
calibration

G. Lichtenberg et al.

SCIAMACHY Level1 data: Calibration concept and in-flight calibration

G. Lichtenberg[1], Q. Kleipool[1,*], J.M. Krijger [1], G. van Soest [1,2], R. van Hees[1],
L. G. Tilstra[2], J. R. Acarreta [2], I. Aben[1], B. Ahlers[4], H. Bovensmann[3],
K. Chance[7], A. M. S. Gloudemans[1], R. W. M. Hoogeveen[1], R. Jongma[1], S. Noël[3],
A. Piters[2], H. Schrijver[1], C. Schrijvers[4,*], C. E. Sioris [7], J. Skupin[3], S. Slijkhuis [5],
P. Stammes [2], and M. Wuttke[3]

[1]SRON National Institute of Space Research, Utrecht, the Netherlands
[2]Royal Netherlands Meteorological Institute (KNMI), de Bilt, the Netherlands
[3]Institute of Remote Sensing (IfE), University of Bremen, Germany
[4]TNO Science and Industry, Delft, the Netherlands
[5]DLR-DFD/IMF, Weßling, Germany
[7]Harvard-Smithsonian Center for Astrophysics (SAO), Cambridge, USA
[*]now at: Royal Meteorological Institute Netherlands (KNMI), de Bilt, the Netherlands

Correspondence to: G. Lichtenberg (lichten@sron.nl)

Title Page

Abstract	Introduction
Conclusions	References
Tables	Figures

◄◄	►►
◄	►
Back	Close

Full Screen / Esc

Print Version

Interactive Discussion

EGU

Title Page

Abstract | Introduction

Conclusions | References

Tables | Figures

◄◄ | ►►

◄ | ►

Back | Close

Full Screen / Esc

Print Version

Interactive Discussion

EGU

Abstract

This paper discusses the basic concept of the calibration of the SCIAMACHY instrument and remaining open issues. SCIAMACHY is a scanning Limb/Nadir spectrometer covering the wavelength range from 212 nm to 2386 nm. It was launched on-board ENVISAT in February 2002. In general the instrument performance is excellent: It performs as tested on ground and there is only very minor degradation in time. The only exception is the unexpected formation of water ice on the infrared channels 7 and 8 that attenuates the signal and a light leak in channel 7. Both effects will be discussed. In the paper we will explain all individual calibration steps needed to come to a wavelength calibrated spectrum of the Earth reflectance. Open points in the calibrations and latest improvements, such as the new radiometric calibration will also be treated.

1. Introduction

In this paper we describe the optical layout of SCIAMACHY (**SC**anning **I**maging **A**bsorption spectro**M**eter for **A**tmospheric **CH**artograph**Y**), its different observation modes and the on-ground and in-flight calibration concept. We also cover unexpected calibration effects encountered in-flight that require adjustments in the data processing. SCIAMACHY is a scanning nadir and limb spectrometer covering the wavelength range from 212 nm to 2386 nm in 8 channels. It is a joint project of Germany, the Netherlands and Belgium and was launched in February 2002 on the ENVISAT platform. The nominal mission life time is 5 years. SCIAMACHY was designed to measure column densities and vertical profiles of trace gas species in the stratosphere and in the troposphere (Bovensmann et al., 1999). It can detect O_3, H_2CO, SO_2, BrO, OClO, NO_2, H_2O, CO, CO_2, CH_4, N_2O , O_2, $(O_2)_2$ and can provide information about aerosols and clouds. In addition to the spectrally resolved measurements of the Earth shine the polarisation of the incoming light is measured with 7 broadband sensors. The Q fraction of the polarisation is measured with 6 sensors approximately covering the spectral

ranges of channel 2–6 and 8. The U fraction of the polarisation is measured with a dedicated sensor around 850 nm. The measurements are used to correct the polarisation sensitivity of the instrument. During the on-ground calibration the polarisation sensitivity and the radiometric sensitivity was extensively measured for a range of scan-
5   ning angles. A dedicated on-board calibration unit that contains a White Light Source (WLS) and a Spectral Line Source (SLS) allows to monitor the instrument during the whole mission. Solar measurements are additionally employed to measure light path degradation (see Noël et al., 2003).

The ESA is responsible for the operational processing of all data from ENVISAT and pro-
10   vides the user with two types of SCIAMACHY data: (1) Level 1 data, which contain the spectrum, polarisation fractions and other information and (2) Level 2 data containing geophysical products like total columns or profiles of atmospheric trace gases. Level 1 data are generated from raw, digital Level 0 data and are split up in Level 1b and Level 1c data. Level 1b data are still uncalibrated, but contain all the necessary infor-
15   mation to do a full calibration. Level 1c data are produced by applying some (or all) calibration steps to Level 1b data. ESA provides a tool to calibrate Level 1b data, but the user can also use third party software or develop software to calibrate the data. Often in this paper we will speak of 'operational' data processing as opposed to "sci-entific" processing. Operational data processing is done by ESA and/or is using official
20   ESA tools, while scientific data products are products that scientists have developed themselves. An example for scientific processing is a software package developed at SRON that produces fully calibrated Level 1c data and already incorporates some of the corrections that will become available operationally only after an update of the ESA data processor . Many scientific Level 2 products have been developed in the mean-
25   time by different research groups, e.g. IfE, KNMI, IUP Heidelberg, SRON and others. The operational processor was mainly developed by DLR-IMF together with ESA.

The operational data processing is currently (spring 2005) being updated from the previous version (5.04) to include the latest calibration algorithms and key data. The implementation of this new calibration will be checked and – if necessary – be adjusted

Back   Close

Full Screen / Esc

Print Version

Interactive Discussion

EGU

until mid-2005. After the revision of the data processing, it is planned to re-process all available data with the new processing chain. Excluded from the current update are important corrections for the IR detectors (see below), partly because no operational algorithm is available at this point in time and partly because other corrections were
⁵ regarded as having a higher priority. The earliest implementation date for additional IR corrections is September 2005. Without these corrections operational products from the IR wavelength range will not be useful, so users must develop their own retrieval algorithm or must make use of trace gas products developed in the scientific community (e.g. Buchwitz et al., 2005; Gloudemans et al., 2005; Frankenberg et al., 2004).
¹⁰   In this paper we give a complete overview of the calibration and problems that still have to be solved. We will also try to give an indication of the effect of calibration problems on retrievals. Since the operational processing chain is currently being updated and no newly processed data are available at this point in time, for some calibration issues only a rough estimate of the effect on Level 2 products can be given. However,
¹⁵ it is the intention of this paper to serve as a future reference for detailed studies into specific calibration issues. The first section describes the different instrument modes and the layout of the instrument. Then the overall calibration concept is discussed in the second section before the individual calibration steps are explained in Sects. 3–7. Section 8 treats unexpected effects that require an adjustment of the calibration proce-
²⁰ dure such as ice in channel 7 and 8 and the light leak in channel 7. Finally a summary of the most important open calibration issues is given.

2. The instrument

SCIAMACHY can observe the Earth, the sun and the moon in various modes. Two scanner modules, the so-called Elevation Scanner Module (ESM) and Azimuth Scan-
²⁵ ner Module (ASM) can be used to direct light into the instrument. Both scanner modules can be rotated a full 360°- and have identical flat, uncoated mirrors mounted on one side and a diffuser mounted on the other side. The scanners enable SCIAMACHY

EGU

to observe in the following modes (see also Noël et al., 2002):

Nadir:. The instrument is looking directly down to the Earth and uses only the ESM mirror. The Instantaneous Field of View (IFoV) is approximately 25 km×0.6 km (along × across track), the typical ground pixel size is 32 km×60 km at a full swath width of 960 km (scanning East–West).
5   Higher resolution is possible in special operation modes.

Limb:. The instrument looks into flight direction using the ASM mirror for East–West scans and the ESM mirror to sample heights from the horizon to an altitude of 93 km in 3 km steps. The IFoV is 103 km×2.6 km (azimuth × elevation) at the tangent point around 3000 km ahead of the satellite. The typical spatial resolution is 240 km×3 km covering 960 km in one East-West
10   scan. The ESM scanner compensates for the curvature of the Earth to keep the same tangent height for each individual East-West scan. At the end of each Limb measurement a dark signal measurement is made at a tangent height of 250 km.

Solar Occultation:. The sun is acquired at sun rise over the Northern Pole and is tracked through the atmosphere from 17 km to the upper edge of the atmosphere. In this mode the
15   small aperture is used to reduce the signal in all channels. Additionally the Neutral Density Filter (NDF) reduces the light in channels 3–6 by a factor of 5.

Solar Irradiance:. In this mode the sun is measured with a mirror diffuser combination (either ASM mirror + ESM diffuser + NDF filter or ASM diffuser + ESM mirror) to obtain a solar reference spectrum

20   *Monitoring:.* In this mode the sun or the moon are observed above the atmosphere in order to measure any degradation of the instrument optical path. In the sun modes the small aperture and the NDF is used. The moon can only be observed for about one week per month above the Southern Hemisphere using both mirrors. The sun can be observed with both mirrors (Limb configuration) or in the so-called sub-solar mode using only the Nadir mirror. Sub-solar
25   measurements are only possible when the satellite crosses the equator on the day side.

Calibration:. SCIAMACHY has its own calibration unit with a 5 Watt Tungsten halogen WLS for instrument monitoring and a PtCrNe spectral line source to perform in-flight spectral calibration. Both lamps can be observed only with the ESM (mirror or diffuser).

EGU

A simplified optical train for all possible modes is shown in Fig. 1. After passing the scanners a 31 mm diameter telescope mirror produces a focus on the entrance slit of the spectrometer. The entrance slit is 180 microns wide and 8 mm high, resulting in an Instantaneous Field of View (IFoV) of 0.045 degrees in the dispersion direction and
5 1.88 deg in the cross-dispersion direction. After the slit the beam is collimated and is directed into the Optical Bench Module (OBM).

The OBM design is based on the double dispersing spectrometer principle. The light is first dispersed by a pre-disperser prism creating an intermediate spectrum. Small pick-off prisms and subsequent di-chroic mirrors direct the light into the 8 so-called
10 science channels. Each of these channels contains a grating for the final dispersion of the light to moderate spectral resolution. At the pre-disperser prism p-polarised light is split off to the Polarisation Measurement Devices (PMDs) through a Brewster reflection. The PMDs are broadband sensors with wavelength ranges that cover approximately the wavelengths measured in channels 2–6 and 8 (see Table 1). Additionally to the
15 6 PMDs A–F measuring Q the PMD 45 measures the U Stokes parameter. The PMDs are non-integrating devices that are read out at 40 Hz. The polarisation of the incoming light can be derived by combining the measurements in the science channels and the PMD measurements as will be explained in Sect. 7.

The science channels of SCIAMACHY employ two types of detectors. For the
20 UV/VIS range (channels 1–5) standard silicon EG&G Reticon detectors with 1024 pixels are used that are sequentially read out in approximately 30 ms. The near IR channels 6–8 employ Indium Gallium Arsenide (InGaAs) detectors manufactured by EPI-TAXX (now owned by JDS Uniphase) with a custom focal plane array designed by SRON (Hoogeveen et al., 2001). All pixels in these detectors are read out in parallel
25 with dedicated amplifiers avoiding problems with spatial aliasing (see below). In order to have sensitivity to wavelengths beyond 1700 nm, the detector material in the longer wavelength part of channels 6 starting at pixel number 794 (called channel 6+) and channels 7 and 8 were doted with higher amounts of Indium leading to a mismatch between the lattice of the InP substrate and the InGaAs light detecting layer. Unfor-

EGU

tunately, this mismatch leads to a number of unusable pixels in these channels (see Sect. 4.2).

In channel 2 the wavelength direction is reversed, i.e. *high* pixel numbers correspond to *short* wavelengths to avoid spatial aliasing in the overlap of channel 1 and channel 2
5 from 310–314 nm and in the overlap of channels 2 and 3 (383–412 nm). Spatial aliasing occurs due to the fact that the detector pixels in channels 1–5 are read out sequentially starting with pixel number 1. Pixels that are read out at a different time see a different ground scene because of the movement of the satellite and the scan mirrors, introducing a wavelength dependent bias into the spectrum. The size of the effect de-
10 pends on the variability of the ground scene. The reversal of channel 2 ensures that the channel overlaps see the same ground scene.

The minimum exposure time of the detectors is nominally 31.25 ms. The IR channels 6–8 can be read out in the so-called "hot mode" allowing much shorter integration times down to 28 μs. Note that the scanning motion of the mirrors and the readout of
15 the detectors are synchronised by pulses with a frequency of 16 Hz (corresponding to 62.5 ms) meaning that at integration times shorter than this frequency, readouts are discarded without being sent to the ground station, e.g. for a 31.25 ms integration time only every second readout is actually available in the data product. However, integration times shorter than 62.5 ms are only used in calibration and monitoring modes.
20 In order to reduce the noise the detectors are cooled with a passive radiative cooler (SCIAMACHY Radiative Cooler, SRC) which has two stages. The first stage provides cooling to channels 1–6 and the second stage to channels 7 and 8. Seasonal variations of the detector temperature are compensated by manual adjustment of the power to three so called trim heaters. Channel 6+, 8 and 5 (in that order) show a significant
25 temperature dependence of their quantum efficiency. The signal in those detectors changes 2-3% per Kelvin depending on the wavelength. Table 1 shows the approximate detector temperature range for the year 2004, excluding decontamination periods. The temperature of the optical bench is actively controlled with a feed-back loop holding the temperature stable at 255.1 K±40 mK over the orbit. The remaining temperature

EGU

variation over the orbit leads to a small change of the background signal in channel 8 (see Sect. 4.2).

Finally, a special feature of the readout of the detectors has to be mentioned. The total integration time in a channel is defined as the product of the Pixel Exposure Time (PET) and a co-adding factor. Co-added data are summed up on-board before they are sent to the ground station. It is possible to assign consecutive pixels to so-called clusters, each having its own co-adding factor, i.e. the integration time in each cluster can be a multiple of the PET in a given channel. The PET is fixed per channel[1]. The cluster concept can be tuned such that the resolution in the spectral windows containing the most important trace gases is the highest. In this way the scientific return can be optimised within the limits of the data rate that is available to SCIAMACHY for sending the data to the ground. A drawback of this concept is that it introduces several complications in the data processing of SCIAMACHY. The observation mode, the cluster definition and the integration time setting constitute what is called a *state*. SCIAMACHY has 70 pre-defined states that cover all Earth observation, monitoring and calibration modes.

3. Calibration concept

The calibration converts electronic signals into physical quantities. The general calibration formula is

$$S_{det} = I(\lambda) \cdot \Gamma_{inst}(\lambda) \cdot QE(T_{det}) + S_{stray} + DC + S_{elec} \tag{1}$$

where S_{det} is the signal measured on the detector, I is the incoming intensity, Γ_{inst} the total transmission of the instrument, $QE(T_{det})$ the detector temperature dependent quantum efficiency, S_{stray} the stray light, DC the total dark signal and S_{elec} electronic

---

[1]Channel 1 and 2 are divided in two parts w.r.t. PETs, i.e. for these channels 2 different PETs are possible.

EGU

effects like non-linearity. This equation holds for every detector pixel. In order to obtain the spectrum as a function of wavelength λ for each pixel the wavelength has to be determined and the equation has to be inverted to calculate the intensity I. Additionally, to get the true shape of the spectrum the instrument specific slit function has to be applied. Generally, the transmission of the instrument is dependent on the polarisation of the incoming light. The individual calibration steps will be explained in more detail in the following sections. First the general concept behind the calibration of the SCIAMACHY instrument is discussed.

The experience of the Global Ozone Measuring Experiment (GOME) on-board the 1995 launched ERS–2 satellite, where various air-vacuum effects led to calibration problems, showed that spectrometers should ideally be calibrated under thermal vacuum (T/V) conditions (see e.g. Aben et al., 2000). In the case of SCIAMACHY a calibration done completely under T/V conditions was not possible, because a range of incidence angles on the mirror(s) and mirror–diffuser combination had to be covered and the vacuum tank was too small to allow the necessary rotation of the instrument. Therefore a combination of T/V and ambient measurements was used. The radiometric sensitivity and the polarisation sensitivity of the instrument were measured under T/V conditions for *one* reference angle and all necessary instrument modes (limb, nadir and irradiance). In order to be able to calibrate all incidence angles on the mirrors (or diffusers), component level measurements of all possible mirror combinations and the mirror-ESM diffuser combination were made under ambient conditions. The ambient measurements were done for a set of angles (including the reference angle measured under T/V conditions) and a set of selected wavelengths. The reference angle measurement is used to transfer the results from the ambient measurement to the T/V measurement. Measurements were done for unpolarised light, s- and p-polarised light and ±45° polarised light. The combination of T/V measurements with the ambient measurements gives ideally the correct instrument response for all incidence angles at begin of life of the instrument. The implicit assumptions for the combination of the T/V and ambient measurements are that the polarisation dependence of the mirrors and

EGU

diffusers are the same in air and in vacuum and that there is no temperature dependence. Both assumptions are reasonable for SCIAMACHY, since uncoated mirrors are used. Critical points in the transfer of ambient and T/V measurements are the geometry (incidence angles on the mirrors or diffusers), the illumination conditions and the

5   detector used in the component measurements. Obviously, errors in the geometry lead to a wrong angle dependence for the calibration quantity to be measured. Light levels during instrument measurements and during component measurements will always be different. While the footprint of the light source on the component can be matched to the footprint during the instrument measurements, it is impossible to re-create the

10   exact illumination conditions. This can introduce systematic errors into the calibration. Finally, care has to be taken that the detector used in the ambient measurements does not introduce artifacts. In order to minimise the effect of the ambient measurement detector, ratios of measurements were used in the ambient calibration where possible.

     In addition to the on-ground calibration measurements, in-flight measurements of the

15   dark signal are performed in every orbit. Changes of the instrument performance in-flight are tracked with internal light sources (WLS and SLS) and solar measurements. For more details on monitoring see e.g. Noël et al. (2003). Details of the calibration are described in the following sections.

4. Detector corrections

20   This section treats corrections related to the electronics of the detectors and the detectors themselves (S_{elec} and DC in Eq. (1)). The UV/VIS channels 1–5 and the IR channels 6-8 have to be treated separately in the calibration due to their different detector material and readout electronics, therefore they will be described separately in this section. The signal in this section is described in terms of Binary Units (BU). The

25   Analog Digital Converter (ADC) of SCIAMACHY codes the signal on the detector in 16 bit meaning that detector signals (or "fillings") are in the range between 0 BU and 65 535 BU.

4.1. Channels 1–5 (UV/VIS)

The first correction that has to be applied is the so-called memory effect (Lichtenberg, 2003). The memory effect was discovered in 1996 during an investigation of the linearity of channels 1–5. In a number of measurements that covered the range from low detector fillings to saturation it was found that the signal deviated from a linear response[2]. The deviation was not dependent on the actual signal level, but on the signal level of the readout done directly *before* (hence the name memory effect). Note that the effect depends on the signal level *including* the analog offset (see below) and dark current. Thus it has to be applied before any other correction. In order to correct for the memory effect, WLS measurements followed by several dark measurements were done on-ground and in-flight. The difference between the first dark measurement after the WLS measurement and subsequent dark measurements gives a correction value as a function of detector filling. This value has to be subtracted from the data to correct for the memory effect. All detector pixels behave in the same manner. The total effect for a single readout is between –0.61% and 0.21% of the detector filling of the previous readout with a maximum effect at fillings around $19\,000\,\mathrm{BU}$–$21\,000\,\mathrm{BU}$, depending on the channel (see Fig. 2). Since the memory effect introduces instrument features that depend on the previous readout, it is not easily possible to make a quantitative estimate of the effect on scientific data. Qualitatively, the memory effect leads to two different kinds of deviations from the "true" spectrum. First, the absolute value of the signal will be wrong, but for measurements that have a reasonable S/N this is not considered a major problem. The second effect, however, is more serious. Since the memory effect changes rapidly as a function of the previous signal for a large range of detector fillings, there is a risk that artificial spectral features are introduced into the measurements. Differential retrieval methods, such as DOAS are very sensitive to changes of the spectral shape of a line, thus the memory effect cannot be neglected. In general

---

[2]Defined by doing a linear fit for all points of up to 90% of the maximum detector filling = $2^{16}-1 = 65\,535$.

the effect on the data is strongest when for a certain spectral region the previous read-out had detector fillings that lead to a high memory effect and the current readout has a very weak signal or when the spectrum shows a high variability in signal levels.

In two cases the memory effect cannot be calculated directly from the available data in a channel. First, if the data are co-added, the individual detector readouts are not available in the data. In this case PMD measurements, which are read out more frequently than the science channels, are used to estimate the signal during the individual readouts in a co-adding sequence. The estimated signals are then used to approximate the total memory effect. Second, each time the instrument changes into a different state (see Sect. 2 for the definition of a state) the mirrors move first into an idle position and then into the position required by the new state. During the movement to the new position the detectors are continuously read out, picking up an unknown signal from the moving mirror. Data from this period are dumped on-board. Thus the previous readout for the first spectrum in a state is not available. The operational processor uses some approximation to estimate the signal during mirror movement, but it is impossible to determine how accurate this approximation is. For this reason we recommend not to use the first readout in a state or, if one does so, carefully inspect the spectrum for artifacts.

The second detector correction that has to be applied is the dark signal correction. The dark signal is measured in every orbit in the eclipse using 5 different states. In channels 1–5 the dark signal consists of two components: the analog offset (AO) and the leakage current (LC). The analog offset is independent of time, it is just a fixed signal added to the measured signal to avoid a negative signal. The leakage current is caused by thermally created electron-hole pairs. The total dark signal for the UV/VIS channels is

$$DC_{UV/VIS} = f_{coadd} \cdot AO + f_{coadd} \cdot t_{PET} \cdot LC \tag{2}$$

where f_{coadd} and t_{PET} are the co-adding factor of the cluster and the pixel exposure time (see Sect. 2). Note that the analog offset is only multiplied with the co-adding

factor since it is time independent but is added to the signal for every detector readout. The dark signal correction is derived in-flight by linear fit to the dark measurements with different integration times. The dark signal in the UV/VIS channels is dominated by the analog offset. The leakage current is only 0.04–0.5 BU/s (Kleipool, 2002) and did not change significantly since launch.

The last detector effect that needs to be characterised is the so-called pixel-to-pixel gain (PPG). If different pixels show a different signal for the same intensity (i.e. if they have a different gain), this can introduce spectral artifacts into the data. Measurements of pixel-to-pixel gain (PPG) showed that all pixels have the same responsivity to light within a factor of 10^{-4}. Thus no correction for the PPG has to be applied for the UV/VIS channels.

4.2. channels 6–8 (IR)

The IR channels do not suffer from the memory effect. However, there is a significant non-linearity that has to be corrected before applying other corrections. The non-linearity has been measured during the on-ground calibration campaign and a correction algorithm was defined (Kleipool, 2003). The maximum non-linearity is around 250 BU, which can be significant for weak absorbers like CO. A separate non-linearity correction for the channels 6, 6+, 7 and 8 has been derived. Within these channels the non-linearity differs for odd and even pixels (starting pixel numbering with 0) because of the different multiplexers used for odd and even pixels. Additionally there is a clear difference in the non-linearity between pixel numbers higher and lower than pixel number 511. This leads to 14 correction curves, four per channel with the exception of channel 6+, which covers only pixels 794 to 1024 (see Sect. 2). Figure 2 shows the non-linearity curves derived for channel 8. The accuracy of the non-linearity correction is around 5–21 BU for detector fillings from 10 000 to 40 000 BU, depending on the channel.

In addition to the non-linearity Channels 6+, 7 and 8 contain a significant number of unusable pixels due to the lattice mismatch between the light detecting InGaAs layer

EGU

and the InP substrate. These pixels are called bad or dead pixels. There are various effects that make these pixels unusable: They could be disconnected pixels preventing any signal readout. Some pixels are so-called Random Telegraph (RT) pixels that spontaneously and unpredictably jump between two levels of dark current leading to
5   different detected signals for the same intensity. Other effects include excessive noise or too high leakage current that saturate the detector. All these effects were measured on-ground and a so-called Bad and Dead pixel Mask (BDM) was created. Pixels in the BDM have to be ignored in any retrieval. Recently it has been discovered that the BDM changes in-flight. The most likely reason is the impact of high energy protons on
10   the detector, a paper is in preparation (private communication, Q. Kleipool, 2004). The effect of the changes of the BDM for CH_4 and CO is described in detail by Gloudemans et al. (2005): It is shown that one bad pixel that is not accounted for can change the CH_4 retrieved total columns by a factor of up to 2. Clearly, the effect on individual retrievals depends on the position of the bad pixel in the retrieval window and on the
15   used retrieval algorithm.

After the application of the non-linearity and the BDM, the dark signal has to be corrected. The dark signal correction in channels 7 and 8 is complicated by the presence of a large thermal background (BG_{th}) and the unforeseen growth of an ice layer on the detector (see Sect. 9.1). The ice layer slowly changes the detector temperature and
20   attenuates the signal on the detector, including the thermal background . The dark signal in these channels becomes

$$DC_{IR} = f_{coadd} \cdot AO + f_{coadd} \cdot t_{PET} \cdot LC + \\ + f_{coadd} \cdot t_{PET} \cdot \Gamma_{ice} \cdot QE(T_{det}) \cdot BG_{th}(\varphi) \tag{3}$$

25   where Γ_{ice} is the transmission coefficient that changes due to the ice layer and $QE(T_{det})$ is the quantum efficiency for the detector. For channels 6+ and 8 the quantum efficiency changes with the detector temperature T_{det}, whereas the first part of channel 6 and 7 show no significant temperature dependence. The thermal background

8938

EGU

is caused by the thermal radiation of the instrument and is the dominant part of the dark signal ($\approx$4000 BU/s) in channel 8. It depends on the orbit phase φ, because the temperature of the instrument is not completely stable, but varies over one orbit due to the changing angle of the solar irradiation. The variation of the dark signal can be up to 60 BU/s which has significant impact on the retrievals of trace gases. Gloudemans et al. (2005) showed a comparison of retrievals with and without the orbital variation results in differences of up to 4% in CH_4 total columns. The orbital variation is measured once a month during a special calibration orbit in which only dark signal measurements are performed by looking to 250 km tangent height in Limb mode. Discussions are under way on how to best implement the orbital variation in the operational processing. The variation of the transmission makes the dark signal correction time dependent meaning that for the channels 7 and 8 a dark signal correction calculated from measurements in the *same* orbit has to be used.

The final detector related correction is the PPG correction. The pixels in the IR do not show the same response to the incoming light. Variations of a few percent can be observed. The PPG is derived by first smoothing a WLS measurement, assuming the spectrum is flat. Then the smoothed spectrum is subtracted from the original measurement, leaving only the high frequent variations that are caused by the different pixel gains in the result. Since the solar measurement is Doppler shifted as a result of the movement of the satellite, the PPG correction needs to be applied *before* any shift of the spectra. It is strictly an effect that is caused by the electronics and the detector and is thus associated to the individual pixels but not to the wavelength. Preliminary investigations by SRON show that the PPG is very stable since launch (private communication, R. Jongma, 2005).

5. Wavelength calibration

The spectral calibration of the SCIAMACHY data is done in-flight using the internal SLS measurements (Slijkhuis, 2000) with the exception of channels 7 and 8 (see be-

low). For selected lines the pixel position is determined using the Falk algorithm (Falk, 1984). The pixel positions are then fitted to theoretical line positions that are part of the calibration data. The polynomial coefficients from the fit are used to calculate the wavelength for each pixel. Measurements of solar Fraunhofer lines are used as a qual-

5   ity check. The wavelength calibration on-ground was done with the internal SLS and additionally with an external SLS except for channels 7 and 8, because in these channels not enough useful lines are available to calculate the wavelength calibration with a sufficient accuracy. In channel 8 this is caused by bad pixels that interfere with the determination of the line position. Channel 7 only contains two strong doublet lines

10 preventing an accurate determination of line positions over the whole channel. In both channels data from on-ground gas cell absorption measurements are used to establish a wavelength calibration

An additional effect discovered during the on-ground calibration is the so-called *blocking shift*: comparison between the external and internal spectral lamp measure-

15 ments on-ground revealed a wavelength shift of up to 0.07 nm. The reason is a partial blocking of the light path during internal SLS measurements. The blocking shift was characterised and is part of the calibration data.

Checks of the spectral calibration in-flight have shown that SCIAMACHY is spectrally very stable. An analysis of on-ground and in-flight (Ahlers, 2004a) data show an abso-

20 lute shift of the wavelength calibration between –0.04 nm in channel 1 to –0.01 nm in channel 3 and the largest shift of 0.07 nm in channel 5. The other channels show no significant shift. The reason for the large shift in channel 5 is unknown. However, since the wavelength calibration is calculated from in-flight data and uses the on-ground data only as an initial starting point the shift will not influence trace gas retrievals. More

25 important is the spectral stability of the instrument. An investigation done after launch by Ahlers (2004a) shows that the spectral stability is better than the requirement of 0.02 pixels/orbit. Possible exceptions are spectral regions near the channel borders, here a detailed investigation has still to be performed. The blocking shift was also verified in-flight by comparing spectral lines positions from the sun-over-diffuser mea-

surements to those of SLS measurements ([Ahlers](#), [2004b](#)). The difference between the wavelength calibration derived from SLS measurements (not applying the blocking shift correction) and sun measurements is up to 0.15 nm, suggesting an increase of the blocking shift. However, the sun measurements show a large spread and the fit used

5 to determine the wavelengths have a lower accuracy. Therefore, it is not clear if the blocking shift has increased or if this is only an artifact caused by the lower fit quality in the sun measurements. Further investigations are needed to clarify this.

6. Stray light

There are two types of stray light (S_{stray} in Eq. ([1](#))), the *spectral* stray light and the

10 *spatial* stray light. Spectral stray light is light of a certain wavelength that is scattered to a detector pixel "belonging" to a different wavelength. It can lead to distortions of the shape of the spectrum. The reason is usually a reflection in the instrument after the dispersion of the light beam. The source of spectral stray light can be within the same channel (intra-channel stray light) or it can scale with the intensity in a different channel

15 (inter-channel stray light). Spatial stray light is light that enters the telescope from outside the IFoV. Spatial stray light is dispersed just as the light from the observation target. Depending on the source of the stray light it can add an additional offset to the spectrum and/or can distort the spectrum, if the primary source of the stray light has spectral characteristics that differ significantly from the observed target. Stray light is

20 usually characterised as a fraction of the total measured intensity for a given pixel.

6.1. Spectral stray light

In a full matrix approach, the spectral stray light determination would measure the stray light contribution from each individual pixel to all other pixels separately. However, practically this is not always possible. In the case of SCIAMACHY a 8192×8192

25 matrix would be needed making the calculation of stray light very slow. Another prob-

lem is that in a full matrix approach the signal per pixel would be too low to measure, since usually only a very small fraction of the incoming signal is stray light. In order to prevent the problems with the full matrix approach the spectral stray light for SCIA-MACHY was separated into three types: (1) Uniform stray light, (2) ghost stray light and (3) channel 1 stray light. Each type of stray light was characterised on-ground using measurements employing a monochromator. A monochromator gives light in a narrow, pre-defined spectral band. The centre wavlength of the spectral band can be adjusted. In the derivation of the stray light fractions from monochromator measurements it is assumed that any signal in detector pixels outside this spectral band is caused by stray light. During the on-ground calibration the spectral stray light was measured by changing the central wavelength of the monochromator spectral band, covering the whole wavelength range of SCIAMACHY. The resulting data are part of the calibration data set and are used to correct the spectral stray light in flight.

The first type of spectral stray light, the uniform stray light, is caused by a diffuse reflection that adds signal to all detector pixels in a given channel. It is by definition not dependent on wavelength. The uniform stray light fraction is calculated in channel 2–8 relative to the average signal in the channel and has values between 0.07% and 0.1% depending on the channel. The relative error of the uniform stray light value from the on-ground calibration is between 15% and 40% of the calculated value, again depending on the channel. Even if the maximum error is assumed, the largest expected stray light fraction is 0.14% which is well within the requirements. It is assumed that the uniform stray light is not dependent on polarisation.

Ghost stray light is caused by a more or less focused reflection of one part of a spectrum to another part of the spectrum. It can distort the shape of the "true" spectrum, because it does not add signal to all pixels. The effect of the ghosts on the retrieval depend very much on the shape and dynamic range of the measured spectrum and are not easily predictable. During the on-ground measurements 15 ghost signals were detected in channels 2–8. The total sum of ghost stray light in a channel is at maximum 1% of the incoming intensity. The current correction does not consider the polarisation

EGU

of the light, an investigation if the polarisation has to be taken into account is planned for the future.

For channel 1 the situation is less favourable with respect to stray light levels. The on-ground measurements showed that the spectral stray light in channel 1 can be up to 10% of the incoming signal. It is also highly wavelength dependent. The main reason for the larger stray light fraction in channel 1 is the high dynamic range of the spectra in this channel, with the lowest signal 3 orders of magnitude smaller than the highest signal. The coarse, artificial separation in uniform and ghost stray light is not sufficient for a correction in channel 1 and an alternative method had to be formulated. The chosen approach combines the correction of uniform and ghost stray light in a modified matrix approach. In order to avoid signal-to-noise problems during the spectral stray light measurements, 10 wavelengths bands were defined separately for s and p-polarised light leading to a total of 20 bands. Nine bands were located in channel 1 to characterise intra-channel stray light and 2 bands covered the signal from channels 2–5 to characterise inter-channel stray light. The channel 1 detector material is not very sensitive for light with wavelengths larger than 1000 nm, so the IR channels do not have to be considered. For each band the stray light contribution to all detector pixels was calculated leading to a 10×1024 matrix for both, s- and p-polarised light. The stray light fraction in channel 1 ranges from less than 1% to as much as 10%. The correction has an accuracy of around 25% and reduces the stray light by an order of magnitude leaving at most 1% stray light in the spectrum after correction.

6.2. Spatial stray light

Spatial stray light is observed in SCIAMACHY limb measurements at altitudes above 90 km and in data taken in Nadir configuration over the North pole. The latter is expected since at that position in the orbit the sun shines directly into the limb port of the instrument producing considerable stray light. In order to minimise stray light above the Pole the ASM is rotated such that the edge of the diffuser/mirror points in flight direction preventing a direct reflection into the telescope. The observed stray light in

this orbit position is caused by remaining reflections of sun light from the baffles and other parts of the Limb port. The stray light in Limb measurements was not expected and was first discovered in measurements taken at 150 km tangent height, where no atmospheric light should be present. These measurements were originally intended to determine the orbital variation of the dark signal in channel 8 (see Sect. 4.2) and as an optional dark correction for the Limb measurements. Investigations (van Soest, 2005) show that the stray light is not caused by a light leak, because spectral structures like air glow emissions and atmospheric absorptions are visible in the measurements, which means that the signal is spectrally dispersed and thus goes through the optics of the instrument. Comparison with MERIS data showed that the stray light does not correlate with the intensity of the scene at the sub-satellite points (the tangent point of the Limb observations is around 3000 km ahead of the satellite), ruling out the possibility that light is entering through the Nadir port and is subsequently directed into the telescope. Measurements of the Limb scans at high altitude and Limb scans at a lower tangent altitude of 10 km show a good correlation confirming that the stray light is caused by light entering the instrument through the slit from regions outside the IFoV. The stray light is highest in channel 2–4 and is very low in channels 1, 5 and 6. The effect of the stray light on the Limb retrievals will be assessed in a future investigation. The Limb scan has been adjusted to take the dark measurement at 250 km instead of 150 km on 26 May 2003 (orbit 6456). At that height the spatial stray light is reduced by an order magnitude to 5–10 BU/s making an estimation of the orbital dark variation possible. However, the dark signal correction of the data should be done with the dark signal derived from eclipse data.

EGU

7. Polarisation

7.1. Theoretical concept

SCIAMACHY is – as all grating spectrometers without a polarisation scrambler – sensitive to the polarisation of the incoming light, i.e. the response will not only depend on the intensity but also on the polarisation of the light. In the polarisation correction the instrument is represented by a so-called Mueller matrix and the light is represented by the Stokes vector (see e.g. Coulson, 1988):

$$\begin{pmatrix} S \\ Q \\ U \end{pmatrix}_{det} = \begin{pmatrix} M_{11} & M_{12} & M_{13} \\ M_{21} & M_{22} & M_{23} \\ M_{31} & M_{32} & M_{33} \end{pmatrix}^{D,P} \begin{pmatrix} I \\ Q \\ U \end{pmatrix}_0 \tag{4}$$

On the left hand side we have the light as detected by the instrument, i.e. in front of the detectors. On the right hand side we have the Mueller matrix $\mathbf{M_{inst}}$ describing the response of the instrument (D denotes the science channels, P the PMD channels) to the incoming light represented by the Stokes vector. The first element of the Stokes vector, I, denotes the total intensity of the light (we use S for the detected signal here). Q is a measure for the polarisation along the x or y-axis of a chosen reference frame and can be described as $Q=I_x-I_y$. U is a measure for the polarisation along the $\pm45°$ direction and is defined as $U=I_{45}-I_{-45}$. Note that the total intensity can be written as $I=I_x+I_y$ or as $I=I_{45}+I_{-45}$. Often Q and U are normalised to the total intensity I, we will denote normalised fractions with q and u in this paper. Note that the formula above is only correct for Earth observations where the circular polarisation of the light V can be neglected. This is usually the case (see e.g. Hansen and Travis, 1974) and thus circular polarisation is not considered in the polarisation correction. All Mueller matrix elements are dependent on wavelength and on the incidence angle of the light on the scan mirror(s) or diffuser. In the calibration ambient measurements on component level and instrument T/V measurements have to be combined meaning that the actual

EGU

instrument matrix has to be calculated by a multiplication of the matrix for the scanner (combination) and the OBM. However, we cannot go into detail in this paper and will use Eq. (4) here. For more information, the reader is directed to Slijkhuis (2000) and Frerick (1999). The Stokes parameters relate in the following way to the polarisation angle χ and the degree of linear polarisation P:

$$\chi = \frac{1}{2} \arctan \left(\frac{U}{Q} \right) \tag{5}$$

$$P = \sqrt{Q^2 + U^2}/I \tag{6}$$

The detectors of SCIAMACHY are only sensitive to the intensity reducing Eq. (4) to

$$S_{det} = M_{11}^D \cdot I \cdot \left(1 + \frac{M_{12}^D}{M_{11}^D} \cdot q + \frac{M_{13}^D}{M_{11}^D} \cdot u \right) \tag{7}$$

where I is the intensity and q and u the polarisation fraction of the incoming light, and S_{det} is the detected intensity. M_{11}^D is the radiometric response function of the science detectors (see Sect. 8) and the reciprocal of the term in brackets is in effect the desired polarisation correction factor. Note that we are leaving out here the so called m-factors that take into account a possible degradation of the light path (see Sect. 9.3). The m-factors correct for each light path long term degradation of the instrument. For details the reader is referred to Slijkhuis (2000).

7.2. Calculation of the polarisation correction

The problem of correcting the response of the instrument for polarisation can be divided into two parts: (1) determining the polarisation sensitivity of the instrument and (2) determining the polarisation of the incoming light in-flight. The polarisation sensitivity was measured on-ground using ratios of measurements as far as it was possible to minimise influences of the measurement set-up on the data. The polarisation reference

Title Page

Abstract	Introduction
Conclusions	References
Tables	Figures

◄ ►

◄ ►

Back Close

Full Screen / Esc

Print Version

Interactive Discussion

EGU

frame used in the calibration is defined w.r.t. the direction of the slit: looking in the direction of the light entering the instrument after the scan mirrors, the +45° polarisation direction is obtained by a 45° clockwise rotation from the p-polarisation direction. The p-polarisation direction is aligned with the long side of the entrance slit of SCIAMACHY.

5 All calibration data are using this reference frame.

SCIAMACHY shows a different sensitivity to s- and p-polarised light and to +45° and −45° polarised light[3]. Thus, in the on-ground calibration measurements with completely s-, p-, 45° and −45° polarised light in ambient and under T/V conditions are used to derive η, the s/p sensitivity of SCIAMACHY and ζ, the −45°/45° sensitivity for Limb and

10 Nadir configuration. Care was taken to ensure that the intensity in all these measurements was the same. The Mueller matrix elements from Eq. (7) relate in the following way to η and ζ:

$$\frac{M_{12}^{D}}{M_{11}^{D}} = \frac{1 - \eta}{1 + \eta} \tag{8}$$

$$\frac{M_{13}^{D}}{M_{11}^{D}} = \frac{1 - \zeta}{1 + \zeta} \tag{9}$$

15 Using Eq. (7) we can define c_{pol} from

$$I = c_{pol} \cdot \frac{S_{det}}{M_{11}^{D}} \tag{10}$$

Combining the above equation with Eqs. (8) and (9) the polarisation correction factor c_{pol} written in terms of the on-ground measurements is

$$c_{pol} = \left[1 + \frac{1 - \eta}{1 + \eta} \cdot q + \frac{1 - \zeta}{1 + \zeta} \cdot u \right]^{-1} \tag{11}$$

---

[3]This is a consequence of a rotation of the polarisation direction of the incoming light by the pre-disperser prism.

with q and u being the polarisation fractions of the incoming light. Note that c_{pol} depends on wavelength, on the scan angle of the mirror(s) and the observation mode, i.e. c_{pol} is different for Nadir and Limb observations.

For the second step, the determination of q and u, the on-board PMDs are used.
5 In on-ground measurements the ratio of the signal in the PMDs and the signal in the science channels was determined for s-, p- and ±45° polarised light for all PMDs. The data processor uses these ratios and additional information to calculate the polarisation of the incoming light. Only a short summary of the polarisation calculation is given here, for details the reader is referred to Slijkhuis (2000). As is clear from Table 1, not
10 the complete wavelength range of SCIAMACHY is covered by the PMDs. The data processor uses theoretical calculations and can optionally also use the channel overlaps in addition to the PMD measurements to determine the polarisation over the whole wavelength range. Roughly the polarisation determination can be divided into two parts, first the calculation of Stokes parameters for individual wavelengths and second the
15 interpolation to the full wavelength grid.

Before the atmospheric polarisation is calculated, a polarisation reference frame has to be defined. The polarisation reference plane used is the local meridian plane containing the satellite, the zenith and the centre of the FOV with the flight direction pointing into the negative y-direction and the z-direction pointing to the instrument. In this ref-
20 erence frame the p-polarisation ($q=-1$) is parallel to the plane and the 45° direction can be obtained by rotating counter-clockwise from the +x-direction to the +y-direction (we will call this the *observation* polarisation frame). This reference frame differs from that used in the calibration making a coordinate transformation necessary. The data processor handles all transformations from the *calibration* reference frame to the *ob-*
25 *servation* frame and v.v. internally. The calculated polarisation fractions in the Level 1 data product are those in the *observation* polarisation frame.

The determination of the polarisation for individual points in the spectrum is done in the following way: The polarisation near 300 nm (where no PMD is measuring) is determined theoretically from the scattering geometry in a single scattering approximation.

The polarisation for the central wavelengths of the PMDs is determined by using the following equation for the signal S_{PMD} in the PMDs

$$S_{PMD} = \sum_{i=\lambda_{start}}^{\lambda_{end}} M_{11}^{P,i} I_{0,i} \cdot \left(1 + \frac{M_{12}^{P,i}}{M_{11}^{P,i}} \cdot q + \frac{M_{13}^{P,i}}{M_{11}^{P,i}} \cdot u \right) \tag{12}$$

with $M_{xx}^{P,i}$ being the Mueller matrix elements as derived from the on-ground PMD cal-
5 ibration for the science channel pixel i covering a certain wavelength and $\lambda_{start,end}$
denoting the wavelength range of the PMD. Note that the PMDs A-F show a weak
sensitivity to u and that the signal of PMD 45 is weakly dependent on q. Therefore,
additional assumptions have to be made to determine q and u from the PMDs. First
the polarisation fractions are determined iteratively from PMD D and PMD 45 (these
10 2 PMDs measure q and u at the same wavelengths)[4]. Then q is determined from the
other PMDs directly. For the determination of u the following assumptions for u/q are
used in the original scheme (but see Sect. 7.3):

- The value of u/q for wavelengths smaller than a pre-defined wavelength $\lambda_{singlesc}$
  is set to the single scattering value assuming in this wavelength range single
15   scattering dominates.

- For wavelengths larger than a wavelength $\lambda_{Aerosol}$ the value of u/q is set to the
  value determined from PMD D and PMD 45 assuming that in this spectral region
  aerosol scattering and clouds dominate the polarisation of the light.

- In between $\lambda_{singlesc}$ and $\lambda_{Aerosol}$ a linear interpolation to the central wavelengths
20   of the PMDs is used.

As already mentioned above, it is also possible to use the channel overlaps to deter-
mine the polarisation. The wavelength range of all channels except channels 6 and 7

---

[4]Note that in the current processor version 5.04 the u value is derived from a theoretical u/q
using the measured q value from PMD D instead of the described approach, see Sect. 7.3.

EGU

and channel 7 and 8 overlap (see Table 1). In the overlaps the same signal is measured, but the polarisation sensitivity is different in the two overlapping channels. One can exploit this difference to determine the polarisation. However, so far q and u values determined from the overlaps are not very realistic. This is possibly related to problems
5   with the low signal in the science channels near the channel boundary and problems with the radiometric calibration in that region (see e.g. Tilstra and Stammes, 2004). In the current data processor version 5.04 the channel overlaps are not used to determine c_{pol}.

The result of the calculations described above are 7 values for q and u, 6 values
10   at the central wavelengths of the PMDs and one single scatter value at 300 nm. The final step in the polarisation algorithm is an interpolation to the full wavelength grid of the science channels to obtain c_{pol} for the whole spectrum. The polarisation fractions for wavelengths between the wavelengths of PMD A and PMD F are calculated by an Akima interpolation (Akima, 1970), the polarisation fractions below 300 nm are set to
15   the single scattering value and the fraction for wavelengths beyond the PMD F wavelength are set to the PMD F value. That leaves the region between 300 and 340 nm. The polarisation degree in this region changes rapidly due to the strong decrease of O_3 absorption. No PMD measurements are available here. In order to obtain the polarisation fractions in this region the so-called Generalised Distribution Function (GDF)
20   which was originally developed for GOME (Aberle et al., 2000) is used. The connection between the wavelength regions where different methods are used is done such that the gradient of the resulting curve remains continuous.

7.3. Problems

Looking at Eq. (11) one limitation of the calibration approach becomes clear. The polar-
25   isation correction is dependent on the accuracy of the q and u determination. The polarisation sensitivity (see Fig. 3) shows spectral features especially in channels 1–3 and in the channel overlaps. Whenever there is an error in the determined polarisation fractions, these spectral features will be visible in the *polarisation corrected* spectra. The

measurement of the polarisation in SCIAMACHY with broadband sensors inevitably introduces an – unknown – error into the polarisation fractions. The spectral features in the polarisation sensitivity will be re-introduced through the polarisation correction, scaled by the error in q and u. A preliminary investigation showed that this is mostly an issue for channels 1–5, where the atmospheric polarisation is relatively high. Since the instrument is more sensitive to the q polarisation fraction, a large error here affects the spectra the most while an error in the u fraction is negligible for most cases. For retrievals large features and features that correlate with a spectral structure of trace gases are most critical, a slow variation over the channel is less critical. channel 1 and 2 show a strong sensitivity and are most susceptible to errors in the polarisation fractions (for an example see Tilstra and Stammes, 2005). A spectral feature of η and ζ around 480 nm in channel 3 prohibits DOAS retrievals of O_3 in that spectral window. Further investigations are planned.

However, not all problems are necessarily related to an error in the determination of the polarisation fraction. Experience has shown that in the past errors in the data processor, in the derivation of the polarisation sensitivities from on-ground measurements and in the conversion of the different polarisation reference frames led to an incorrect polarisation correction. The processor and the calibration data were reviewed by SRON, DLR, TPD and IfE and both were corrected where necessary. Still, there are a few remaining problems. A check of the derived polarisation fractions shows that the values derived from PMD A for limb configurations are still unphysical for some observation geometries (see Fig. 4, bottom). In addition, with the current calibration data and processor version 5.04 it is not possible to derive correct u values (see Fig. 4, top), thus it was decided not to use the original approach as it is described in the previous section to determine u. Schutgens et al. (2004) show that an approach based on the single scatter value of the polarisation leads to good results for most observation geometries and ground scenes. Therefore, the current version of the data processor determines u/q from a single scattering approach for the whole wavelength range to calculate a $u_{singlesc.}$ until the reason for the unphysical u values determined from PMD 45 and

EGU

PMD D is found. The cause of the unphysical values and the impact on retrievals is not clear, investigations are on-going.

The polarisation correction in the IR (PMD F) suffers from the transmission loss due to ice in these channels (see Sect. 9.1), since the polarisation fractions are determined using the ratio between the signal in the science channels and the PMDs. A correct retrieval requires a correction of the transmission in the IR channels. This is not yet implemented in the data processor. Therefore, it is recommended not to use the polarisation correction in the IR. Since the polarisation in that wavelength range is relatively weak, the impact of not correcting for the polarisation sensitivity of the instrument is expected to be moderate.

An additional problem in the polarisation correction algorithm is related to the cluster concept (Tilstra et al., 2005). Jumps in the reflectance spectrum can appear between clusters with different integration times when it is normalised to the integration time. The polarisation at shorter integration times is generally not as good as for longer integration times, because information from the missing parts of the spectrum in the channel is needed for a successful correction. This information has to be approximated for short integrations, since data from clusters with a longer integration time are not available in every readout. This can lead to an erroneous polarisation correction causing jumps at cluster boundaries.

In the meantime, alternative polarisation correction methods for the UV have been proposed by Tilstra and Stammes (2005) and Hasekamp et al. (2002). These methods incorporate the polarisation sensitivities η and ζ themselves to determine a correction for the polarisation.

[EGU](#)

8. Radiometric calibration

8.1. Concept and on-ground measurements

The final step in the calibration of the data is the radiometric calibration. The retrieval of trace gases usually uses the reflectance, the ratio of Earth shine and solar irradiance. The solar irradiance is measured with on-board diffusers in-flight. Using Eqs. 7 and 11 the reflectance can be written as

$$R = \frac{\pi \cdot I_{Earth}}{\mu_0 \cdot I_\odot} = \pi \cdot \frac{S_{det}^{Earth} \cdot c_{pol}}{\mu_0 \cdot M_{11}^{N,L}} \cdot \frac{M_{11}^\odot}{S_{det}^\odot} \tag{13}$$

with $I_{Earth,\odot}$ and $S_{det}^{Earth,\odot}$ as the Earth and sun intensity and measured signal, μ_0 the cosine of the solar zenith angle, $M_{11}^{N,L}$ the radiometric response for limb (L) and nadir (N) and $M_{11}^\odot$ the radiometric responses for sun-diffuser measurements. For a proper calibration the instrument responses have to be determined as a function of wavelength λ and incidence angle α. As already mentioned in Sect. 3 the radiometric response was measured on instrument level under T/V conditions and the mirror (combination) and the mirror diffuser combination were measured under ambient conditions. In order to transfer ambient measurements to T/V measurements the ratio of a T/V measurement to an ambient measurement at the same incidence angle, the reference angle α_0 is used:

$$C_A(\lambda, \alpha_0) = \frac{\mathcal{R}(\lambda)}{\eta_{OBM}(\lambda) \cdot R_s^N(\lambda, \alpha_0) + R_p^N(\lambda, \alpha_0)} \tag{14}$$

where $\mathcal{R}$ is the radiometric response measured under T/V conditions in nadir configuration, η_{OBM} is the polarisation sensitivity of the OBM without the scan mirrors and $R_{s,p}^N$ is the reflectivity of the nadir mirror for s- and p-polarised light. Using this relation,

8953

EGU

the radiometric response for Earth observations and sun observations can be written down as

$$M_{11}^{N,L}(\alpha) = C_A \cdot [\eta_{OBM} \cdot R_s^{N,L}(\alpha) + R_p^{N,L}(\alpha)] \tag{15}$$

$$M_{11}^{\odot}(\alpha) = C_N \cdot C_A \cdot [\eta_{OBM} \cdot \eta_N \cdot B_s(\alpha) + B_p(\alpha) \tag{16}$$

5 where α is the incidence angle on the mirror and diffuser, C_N is a factor that corrects for the Neutral Density Filter (NDF) that is in the light path for sun measurements, η_N is the polarisation sensitivity of the NDF and $B_{s,p}$ is the reflectivity of the combination ASM mirror + ESM diffuser. Note that all elements of the above equations are wavelength dependent. The term in brackets in the above equations constitutes the so-called scan-
10 angle correction, which is derived from ambient measurements.

It was already mentioned that SCIAMACHY can measure the solar spectrum in two ways: Using the ESM diffuser (this is the originally foreseen way) and using the ASM diffuser. The ESM diffuser showed large spectral features of (1–3%) in on-ground measurements. Model calculations predicted that the retrieval of many products (e.g. BrO,
15 SO_2 or OClO) with DOAS could be made impossible by the spectral features (de Beek and Bovensmann, 2000). An analysis of in-flight data was done by Ahlers et al. (2004) and confirmed the presence of spectral features. The ASM-diffuser has been installed at a later stage on the back side of the mirror, after investigations of on-ground measurements revealed the presence of the spectral features. This diffuser is manufactured
20 differently from the ESM diffuser leading to much smaller spectral features. No absolute calibration of the ASM diffuser could be performed, because SCIAMACHY was already integrated with ENVISAT at that time. Preliminary investigations showed that DOAS retrievals are significantly improved by using the ASM diffuser (see e.g. Sierk, 2003). It is therefore recommended that DOAS type retrievals use sun measurements
25 obtained with the ASM diffuser.

SCIAMACHY calibration

G. Lichtenberg et al.

Title Page

Abstract	Introduction
Conclusions	References
Tables	Figures

| ◀ | ▶| |
| ◀ | ▶ |

| Back | Close |

Full Screen / Esc

Print Version

Interactive Discussion

[EGU](#)

8.2. Problems

Shortly after launch comparisons of modeled sun spectra from Kurucz (1995) and measured sun spectra showed that the solar irradiance measured with SCIAMACHY was around 10% too high for all wavelenghts (see e.g. Skupin et al., 2003; Gurlit et al.,
5   2004). The reflectance on the other hand was around 10–20% too low as comparisons with GOME (Tilstra et al., 2003; Latter et al., 2003), MERIS (Acarreta and Stammes, 2005) and radiative transfer models (van Soest et al., 2005) showed. The cause of the deviations could be traced back to the scan angle correction derived from the ambient measurements: in the daily solar irradiance measurements in-flight 30 individual
10 spectra of the sun are taken. During these measurement the incidence angles on the diffuser change due to the movement of the satellite relative to the sun. In the on-ground calibration campaign a set of measurements with the same incidence angles as in the *first* in-flight ESM diffuser sun measurement were done. These measurements were not used for the radiometric calibration. The sun irradiance derived from these
15 data came close to known standards (Ahlers, 2003). The radiometric calibration used data measured with a different geometry not matching the in-flight incidence angles and was relying on the scan angle correction from ambient data. The investigation by Ahlers (2003) and other investigations showed that the scan angle correction did not work for the mirror-ESM diffuser combination and also that absolute value of the re-
20 flectivity $B_{s,p}$ (see Eq. (16)) was not correct. Although DOAS type retrievals do not rely on the absolute values of the reflectance, the retrieval of the aerosol optical thickness, cloud fraction algorithms, the determination of the surface albedo and vertical ozone profiles from nadir need radiometrically accurate data. Without a proper correction to the radiometric calibration these products loose accuracy.
25   The reason for the inadequate scan angle correction and the wrong absolute value of $B_{s,p}$ is unclear. It could be either an error in the algorithms that were used to calculate $B_{s,p}$ from the ambient measurements or not all effects of the measurements set-up were taken into account. It is conceivable that the illumination conditions during the

EGU

measurements made for $B_{s,p}$ were different from those that are encountered in-flight or that detector effects were not fully corrected (the ambient measurements were done on component level, not using the instrument detectors). SRON will do a complete review of the on-ground calibration and the used algorithms to find possible errors.

5   In order to provide useful data before the review is finished, a new radiometric calibration data set was calculated by IfE (Noël, 2005) with input from SRON and TPD. TPD provided a new scan angle correction for $B_{s,p}$ (Schrijvers, 2004) and the raw, on-ground measurement data, SRON provided the new non-linearity (Kleipool, 2003) and memory effect correction (Lichtenberg, 2003) and an in-flight derived NDF transmis-
10 sion. IfE calculated from these inputs new calibration data, improving the interpolation of the ambient data to the full grid, correcting an apparent error in the ambient characterisation of the limb reflectivity $R_{s,p}^L$ and incorporating a new absolute value for the reflectivity $B_{s,p}$. Two different calibration data sets were calculated in this way, using two different types of on-ground data, the "spectralon data" measured with a NIST cali-
15 brated FEL lamp and the "NASA sphere" data measured with an internally illuminated, $BaSO_4$ coated sphere already used in NASA's SBUV and TOMS programs for absolute radiometric calibration. Both calibration data sets were tested by KNMI in September 2004 using a set of 3 reference orbits.

The result of these tests were

20 – both new calibration data sets improve the offset value of the reflectance, the comparison with MERIS and Doubling-Adding KNMI (DAK) radiative transfer model show a deviation within around 5%

– the new calibration data introduce spectral features, especially around 350 nm (not polarisation related) and 880 nm

25 – the spectralon data show better results than the NASA sphere data

On the basis of these results the new spectralon calibration data will be implemented in the data processing update. Further verification and validation will be performed

EGU

to assess the quality of the new calibration and to assess the impact of the spectral features introduced.

9. In-flight effects

9.1. Ice in channels 7 & 8

Shortly after the very first cooling of the detectors, a significant loss of transmission in channel 7 and 8 was discovered. Investigations showed that an ice layer growing on top of the cylindrical lens covering the detectors was responsible. Only channel 7 and 8 are affected because these channels are cooled down to around 145 K while the other channels have temperatures of 200 K or higher (see Table 1). A likely source of the contamination is the carbon fibre supporting structure of ENVISAT itself, since it is known that carbon fibres can accumulate a substantial amount of water. The water contained in the fibres started to gas out once the satellite was in orbit. SCIAMACHY is covered by a double layer of multilayer insulation (MLI) blankets, one from ENVISAT and one from the instrument itself to prevent strong thermal gradients while in orbit. The MLI has a number of venting holes to allow the outgassing of the instrument and prevent a contamination of surfaces, but apparently the venting volume allowed by the holes is not large enough or the holes are obstructed. Thus, the contaminant is not (or too slowly) removed from the instrument volume. Other instruments on ENVISAT have also reported problems due to contamination (see e.g. Perron, 2004; Smith, 2002).

Under the assumption that the ice layer consists purely of water ice the layer thicknesses can be calculated using an absorption coefficient from Grundy and Schmitt (1998). The ice layer thickness is up to 230 μm (600 μm) in channel 7 (channel 8) after six months. In order to remove the ice from the detectors and to restore the transmission, regular decontaminations are performed. The only heater on board with enough power to heat the detectors sufficiently is the decontamination heater that was originally intended to decontaminate the radiative cooler of the detectors every 6 months.

[EGU](#)

The drawback of using this heater is that it is not possible to heat channels 7 and 8 separately from the other channels, the heating always raises the temperatures of all channels leading to a substantial loss of data quality during decontamination periods. In order to properly remove all the ice from the detectors and their immediate vicinity, a decontamination period of 300–370 h has been found to be most effective. During a decontamination the detector temperatures are raised to about 280 K. The OBM is also heated to around 265 K to prevent ice settling on OBM elements. After each decontamination the transmission is fully restored. The growth of the ice layer in channel 8 is shown in Fig. 6. The calculation of the layer thickness was done for spectral bins of 64 detector pixels with the appropriate absorption for each wavelength bin. In both channels the ice layer is thicker at the beginning of the channel (the blue end) than at the end of the channel at higher wavelengths. The reason for this is unclear, since the thermal coupling from the detector to the cooler is in the middle of the channel, one could maybe expect the ice layer to be thickest in the middle of the channel, if the thermal gradients over the detector array were strong enough.

The long term development of the transmission in both channels is very different. While channel 8 shows more or less the expected behaviour with an exponential decay of the transmission after each decontamination when the ice layer starts to grow again, channel 7 shows a somewhat erratic behaviour (see Fig. 7). After the decontaminations in August 2003 (black x's) and June 2004 (blue triangles) the transmission declined very rapidly in a linear fashion to reach a minimum after around 20 days. Then the transmission went slowly up again. In January 2004 (blue crosses) and 2005 (red diamonds) a completely different behaviour can be seen with constant transmission at a very high level. The reason for the erratic behaviour of channel 7 is not known. One hypothesis is that a second cold trap resides somewhere in channel 7. This second cold trap is sometimes triggered and collects the majority of ice before it can settle on the detector lens. However, this explanation is purely based on the observed transmission behaviour of channel 7 and up to now no part of the detector module could be clearly identified as a possible second cold trap. The different behaviour of channel 7

EGU

and 8 is also puzzling: since both channels are of identical design and have almost the same temperature (the difference is around 1K), one would expect a similar behaviour.

Regardless of the reason of the ice layer build-up and its behaviour over time, the calibration and the operations of SCIAMACHY have been adjusted to minimise the effect of the ice. The first adjustment were made to the decontamination frequency. Originally it was required to decontaminate the cooler at least every six months to prevent irreparable damage to the cooler. However, the in-flight experience has shown that the cooling power did not decrease in 3 years of operations. Therefore it was decided to only do a decontamination, when the transmission in channel 7 and 8 drop below a level where a useful retrieval is no longer possible. This prevents a situation like in summer 2004, were the transmission in channel 7 was degraded by 60% on a short term and by 40% in the long term by the decontamination (blue triangles in Fig. 7). Apart from this operations adjustment, the ice layers lead to the following effects that can affect trace gas retrieval (see also Gloudemans et al. (2005)):

Signal-to-noise loss due to transmission loss:. When a sun reference from the same day is used, the effect on the value of the reflectance is only minor since the transmission loss cancels in the ratio of Earth and solar spectrum. However, the overall signals are lower leading to a lower signal-to-noise-ratio.

Change of slitfunction:. The slit function is changed significantly by the scattering ice layer on the detector. This scattering is dependent on the thickness of the ice, which is not equal over the detector array (see above). A correction scheme using known trace gas contents for a certain location is presented in Gloudemans et al. (2005) as well as the effect on the retrieval if the slit function is not corrected.

Change of the dark signal:. The dominant part of the dark signal in channel 7 and 8 is the thermal background (see Sect. 4.2). The thermal background gets attenuated by the ice just like any other signal on the detector, leading to a variation of the dark signal on the timescale of a few orbits. Thus the IR data have been corrected with a dark measured as close as possible to the trace gas measurements. This has been implemented in the data processing in 2004 (version 5.01). In addition, the orbital variation of the background in channel 8 will also change with the transmission. It is currently investigated if this affects retrievals in channel 8.

[EGU]

Change of detector temperature:. The ice also covers the gold plated aluminium structures of the detector suspension. The ice increases the infrared absorption properties and thereby the radiative heating of the detectors. As a result the detector temperature increases slowly. Values directly after a decontamination are around 0.05 K/day going down to 0.02 K/day as the
5   transmission stabilises. The detected signal in channel 8 will change because the quantum efficiency in this channel is dependent of the temperature. However for most purposes this effect is minor compared to the overall effects of the ice.

9.2.   Light leak in channel 7

After launch it was discovered that channel 7 shows a spurious signal in Limb dark
10   measurements that is much higher than the spatial stray light found in the other chan-
nels (see Sect. 6.2). The signal has no spectral signature, but is a broadband feature. This excludes that it is caused by light that goes through the optics of the instrument. Further investigations were done by SRON to characterise the light leak. In this study, we have used limb dark measurements at 250 km from all available Level 1b data of
15   February 2004 to evaluate the light leak of channel 7. In order to determine the true signal of the light leak, the data were corrected for non-linearity, dark signal (derived from the eclipse part of the orbit) and spectral stray light.

Figure 8 shows the residuals after correction, i.e. the signal caused by the light leak and mean absolute deviation (BU/s) indicating the variation of the light leak as derived
20   from the data set. The upper panel shows the median of the residuals as a function of orbit phase for pixel 103, 502, and 835, indicated by triangles, boxes and stars, re-
spectively. The lower panel shows the mean absolute deviation for the same pixels. The statistic analysis of the dataset shows clear evidence for the presence of a light leak. The derived light leak correction is spectrally smooth, and shows a systematic
25   behavior as function of orbit phase. However, the residual errors σ_{adev} are very large ($\approx$50 BU/s), nearly comparable to the size of the light leak signal. Therefore, the light leak is not (only) a function of orbit phase and more likely a function of viewing geome-
try combined with the presence of regions with high albedo, maybe caused by clouds.

Title Page

Abstract | Introduction

Conclusions | References

Tables | Figures

◄ | ►

◄ | ►

Back | Close

Full Screen / Esc

Print Version

Interactive Discussion

[EGU](#)

Up to now no set of parameters could be found to characterise and correct the light leak with sufficient quality. Before such a set is found, a correction of the light leak is impossible, hampering all retrievals in this channel. It is not clear what the impact of the light leak on retrievals in channel 7 is. To the authors knowledge no retrieval in channel 7 has been attempted so far. Possible products in this channel are temperature profiles, cloud fractions and CO_2 total columns. It is very likely that most retrievals will be severely affected because of the size of the light leak and its erratic behaviour. Clearly, further study to understand the cause of the light leak and to develop a correction is needed.

9.3. In-flight degradation monitoring

We will give only a short summary of the monitoring here. Details of the application of the monitoring to the calibration can be found in Slijkhuis (2000) and first results are described by Noël et al. (2003). Preliminary monitoring results can be found at http://www-iup.physik.uni-bremen.de/sciamachy/LTM/LTM.html. The correction of a given light path is done by comparing calibration and monitoring measurements to the same measurement at a chosen reference point. The results are the so-called m-factors, which are incorporated in the Level 1 files and used in the calibration of the data. At the moment of this writing not enough Level 1 data of sufficient quality are available to do a proper monitoring, therefore a preliminary monitoring is done on the basis of Level 0 files. The results show that the UV channels 1 and 2 show an average degradation of the transmission of around 10% in the 3 years since launch. All other channels show a stable transmission except for channel 7 and 8, where the ice layer leads to a transmission loss in between the decontaminations. A first look into the spectral dependency of the degradation seems to indicate that the channel edges and the regions with a high polarisation sensitivity degrade the fastest. However, further studies are needed to confirm these results.

[EGU](#)

10.   Conclusions

In this paper we have described the basic concepts of the calibration of the SCIA-MACHY instrument on-board ENVISAT. The calibration uses a combination of on-ground T/V and ambient measurements and a number of in-flight measurements. The individual calibration steps as well as problems in the SCIAMACHY calibration have been discussed. The instrument itself has shown in general an excellent performance in the last 3 years. No hardware problems were encountered and the in-orbit per-formance has not changed much with respect to the on-ground calibration. Notable exceptions are the ice in channels 7 and 8, which is a problem that SCIAMACHY shares with two other instruments on the ENVISAT platform and the light leak in chan-nel 7. Several errors in the on-ground calibration and the data processing were found in the last years, a large number of which will be corrected in the current update of the processing chain. After the update, the level 1 data will be significantly improved. Summarising, the following points can be made:

Memory effect:. This effect is only seen in channels 1–5 and is an additive correction. Its effect on the retrieval is difficult to predict, but consecutive measured spectra of a highly variable scene and spectra with a high dynamic range are most likely to be affected. An updated version of the memory effect correction will be implemented during the current update of the operational processor.

Non Linearity:. This effect is only seen in channels 6–8 and is an additive correction. The effect on the retrieval is expected to be minor. Only the retrieval weakly absorbing trace gases is assumed to be affected. The non linearity correction will be implemented during the current update of the operational data processor.

Bad and Dead Pixels:. Bad and dead pixels have to be masked out for retrievals, because pixels of this kind can ruin the retrieval of trace gases. Recently it has been discovered that the number of bad and dead pixels does change in-flight. The original calibration concept did not foresee a frequent update of the bad and dead pixel mask. Discussions between SRON and ESA have started on how to best implement a regular update of the mask into the operational processing.

Dark correction:. The dark correction in channels 1–6 did not show strong variation since launch. In the channels 7 and 8 the dark correction changes every orbit, because of the ice layer growth. These channels need a dark correction derived from an orbit measured as close as possible in time to the science measurement. Since March 2004 the operational processor
5 (version 5.01) uses the closest available dark measurement in the dark correction.

Orbital variation of darks:. channel 8 shows an orbital variation of the dark signal caused by minute changes of the OBM temperature. The orbital variation has a significant impact on CH_4 retrievals and has to be taken into account in the retrieval. It will be implemented during the current update of the operational data processor.

10 *Changes caused by ice:.* The growing ice layer in channels 7 and 8 leads to a decrease of the transmission. A lower signal-to-noise ration in the reflectances is the result. A correction of the transmission is straight-forward, but not yet implemented in the operational processing. More detrimental to trace gas retrievals is the change of the instrument slitfunction caused by scattering of the incoming light by the ice layer. While SRON developed a slit function correction
15 based on scenes with known trace gas content, it is not possible to implement this algorithm in the operational processing. An operational processing is not available at this moment. The operations of the instrument now include regular decontaminations to remove the ice.

Light leak channel 7:. The spurious signal caused by the light leak can be as high as 120 BU/s. While some dependence of the signal on the orbit phase can be seen, the variation over time
20 can be as high average light leak signal itself. Due to the erratic nature of the signal, no correction algorithm could be developed so far. The light leak will severely affect all retrievals in this channel.

Spectral calibration:. SCIAMACHY is spectrally very stable with the possible exception of the channel overlap, where a detailed investigation is needed.

25 *Stray light:.* Apart from channel 1 the amount of spectral stray light is very low. A dedicated stray light correction for channel 1 is implemented in the processing and is able to reduce the stray light to around 1% of the incoming intensity for individual pixels. Spatial stray light was discovered in Limb observations. Investigation showed that the stray light is entering through the slit from regions outside the IFoV. The impact of the spatial stray light on retrievals and a
30 possible correction has still to be investigated.

Title Page

Abstract | Introduction

Conclusions | References

Tables | Figures

◄ | ►

◄ | ►

Back | Close

Full Screen / Esc

Print Version

Interactive Discussion

EGU

Polarisation correction:. A conceptual limitation of the polarisation correction used in the calibration is the sensitivity to errors in the retrieved q and u values. Spectral features in the polarisation sensitivity η and ζ will be introduced through the polarisation correction when the polarisation fractions are wrong. The size of the effect depends on the polarisation degree and the size of the error. Channels 1–3 are most sensitive to this kind of error. The currently implemented polarisation correction is not able to retrieve a physical value for u from the PMD D/PMD 45 combination, therefore a value for u determined from the single scattering approximation is used in the determination of the correction factor c_{pol}. For some cases the polarisation fraction determined with PMD A in limb are unphysical. While a systematic study is missing, results show that the polarisation correction does not always remove all polarisation effects from the data. The correction was reviewed during the last year and improvement and bug fixes are implemented during the current update of the processor. After the implementation is finished, a new verification of the polarisation correction is planned.

Radiometric calibration:. The basis of most retrievals is the ratio of Earth shine to solar irradiation. SCIAMACHY can measure the solar irradiation with two diffusers, mounted on the ESM and the ASM. Preliminary studies showed that the ASM diffuser is more suitable for DOAS type retrievals than the ESM diffuser. The ASM diffuser is not radiometrically calibrated, while the ESM diffuser is. However, the original radiometric calibration produced solar spectra that were up to 10% too high and reflectances that were 15–20% too low. Newly calculated radiometric calibration data reduce this offset, producing reflectances that are good within 5%, but they also introduce spectral features. Usually retrievals that need an accurate reflectance are not as sensitive to spectral features as DOAS type retrievals, but it has to be investigated, if this is a valid assumption for the introduced spectral features. The new radiometric calibration data are incorporated in the current update and investigations on how to improve the radiometric further are going on.

SCIAMACHY calibration

G. Lichtenberg et al.

Title Page

Abstract	Introduction
Conclusions	References
Tables	Figures

◄ | ►|

◄ | ►

Back | Close

Full Screen / Esc

Print Version

Interactive Discussion

EGU

References

Aben, I., E., Eisinger, M. H., Snel, R., and Tanzi, C.: GDAQI Final Report, TN-GDAQI-003SR/2000, Tech. rep., ESA/ESRIN, 28–57, 2000. 8933

Aberle, B., Balzer, W., von Bargen, A., Hegels, E., Loyola, D., and Spurr, R.: GOME Level 0 to 1 Algorithms Description (ER-TN-DLR-GO-0022), Tech. Rep. 5a, DLR, http://atmos.af.op.dlr.de/cgi-bin/h.cgi?page=projdocs, 2000. 8950

Acarreta, R. J. and Stammes, P.: Calibration Comparison between SCIAMACHY and MERIS onboard ENVISAT, IEEE Geosc. and Rem. Sens. Letters, 2, 31–35, 2005. 8955

Ahlers, B.: Investigation of the sun irradiance offset in comparison with standard sun irradiances (TPD-SCIA-PhE-TN-10), Tech. rep., TNO, 24-39, 2003. 8955

Ahlers, B.: Comparison of SLS and WLS calibration measurements on-ground and in-flight (TPD-SCIA-PhE-TN-013), Tech. rep., TNO, 2004a. 8940

Ahlers, B.: Performance verification of spectral shift by vignetting of SLS (TPD-SCIA-PhE-015), Tech. rep., TNO, 2004b. 8941

Ahlers, B., Bazalgette Correges-Lacoste, G., Schrjvers, C., and Brug, H.: In-orbit detection of spectral features in SCIAMACHY, in Sensors, Systems, and Next Generation Satellites VIII, vol. 5570 of Proc. SPIE, 401–410, 2004. 8954

Akima, H.: A new method of interpolation and smooth curve fitting based on local procedures, J. ACM, 17, 589–602, 1970. 8950

Bovensmann, H., Burrows, J. P., Buchwitz, M., Frerick, J., Noël, S., Rozanov, V. V., Chance, K. V., and Goede, A. P. H.: SCIAMACHY: Mission objectives and Measurement Modes, Atmos. Sci., 56, 127–150, 1999. 8926

Buchwitz, M., de Beek, R., Noël, S., Burrows, J. P., Bovensmann, H., Bremer, H., Bergamaschi, P., Körner, S., and Heimann, M.: Carbon monoxide, methane and carbon dioxide columns retrieved from SCIAMACHY by WFM-DOAS: year 2003 initial data set, Atmos. Chem. Phys. Discuss., 5, 1943–1971, 2005, SRef-ID: 1680-7375/acpd/2005-5-1943. 8928

Coulson, K. L.: Polarisation and intensity of Light in the atmosphere, A. Deepak, Hampton, Va., USA, 1–28, 548–551, 1988. 8945

de Beek, R. and Bovensmann, H.: Impact of SCIAMACHY Diffuser Spectral Characteristics on Level 1–2 DOAS Products, Tech. rep., IfE, 2000. 8954

Falk, W. R.: Data Reduction from Experimental Histograms, Nuclear Instruments and methods

EGU

in Physics Research, 220, 473–478, 1984. 8940

Frankenberg, C., Platt, U., and Wagner, T.: Retrieval of CO from SCIAMACHY onboard EN-VISAT: detection of strongly polluted areas and seasonal patterns in global CO abundances, Atmos. Chem. Phys. Discuss., 4, 8425–8438, 2004,
    SRef-ID: 1680-7375/acpd/2004-4-8425. 8928

Frerick, J.: How to generate phase shift corrected greek key data (IFE-TN-211299), Tech. rep., IfE, 1999. 8946

Gloudemans, A. M. S., Schrijver, H., Kleipool, Q., van den Broek, M. M. P., Straume, A., Licht-enberg, G., van Hees, R. M., Aben, I., and Meirink, J. F.: The impact of SCIAMACHY near-infrared instrument calibration on CH_4 and CO total columns, Atmos. Chem. Phys. Discuss., 5, 1733–1790, 2005,
    SRef-ID: 1680-7375/acpd/2005-5-1733. 8928, 8938, 8939, 8959

Grundy, W. M. and Schmitt, B.: The Temperature-dependent Near-Infrared Absorption Spec-trum of Hexagonal H_2O ice, J. Geophys. Res. E., 103, 25 809–25 822, 1998. 8957

Gurlit, W., Bösch, H., Bovensmann, H., Burrows, J. P., Butz, A., Camy-Peyret, C., Dorf, M., Gerilowski, K., Lindner, A., Noël, S., Platt, U., Weidner, F., and Pfeilsticker, K.: The UV-A and visible solar irradiance spectrum: inter-comparison of absolutely calibrated, spectrally medium resolution solar irradiance spectra from balloon- and satellite-borne measurements, Atmos. Chem. Phys. Discuss., 4, 8439–8469, 2004,
    SRef-ID: 1680-7375/acpd/2004-4-8439. 8955

Hansen, J. E. and Travis, L. D.: Light scattering in planetary atmospheres, Space Science Reviews, 16, 527–610, 1974. 8945

Hasekamp, O. P., Landgraf, J., and van Oss, R.: The need of polarization modeling for ozone profile retrieval from backscattered sunlight, J. Geophys. Res. D (Atmospheres), 123, 4692, doi:10.1029/2002JD002387, 2002. 8952

Hoogeveen, R. W. M., van der A, R. J., and Goede, A. P. H.: Extended wavelength InGaAs infrared (1.0–2.4 μm) detector arrays on SCIAMACHY for space-based spectrometry of the Earth atmosphere, Infrared Physics & Technology, 42, 1–16, 2001. 8930

Kleipool, Q.: SCIAAMCHY SODAP; Objective 38: Leakage current versus temperature (SRON-SCIA-PhE-RP-006), Tech. rep., SRON, http://www.sron.nl/~SCIA_CAL/SCIACALdocuments.php, 2002. 8937

Kleipool, Q.: SCIAMACHY: Recalculation of OPTEC 5 Non-Linearity (SRON-SCIA-PhE-RP-013), Tech. rep., SRON, http://www.sron.nl/~SCIA_CAL/SCIACALdocuments.php, 2003.

Title Page

Abstract | Introduction

Conclusions | References

Tables | Figures

◄ | ►►

◄ | ►

Back | Close

Full Screen / Esc

Print Version

Interactive Discussion

EGU

8937, 8956

Kurucz, R.: The solar spectrum: atlases and line identifications, in: Laboratory and Astronomical High Resolution Spectra, edited by: Sauval, A., Blomme, R., and Grevesse, N., vol. 81 of Astron. Soc. of the Pacific Conf. Series, 17–31, 1995. 8955

5 Latter, B. G., Siddans, R., and Kerridge, B. J.: Intercomparison of Reflectances Observed by SCIAMACHY, GOME, AATSR and ATSR-2, EGS–AGU–EUG Joint Assembly, Abstracts from the meeting held in Nice, France, 6–11 April 2003, abstract #11451, 2003. 8955

Lichtenberg, G.: SCIAMACHY channel 1-5 Memory Effect I: Key data implementation and in-flight measurements (SRON-SCIA-PhE-RP-11, issue 2), Tech. rep., SRON, http://www.sron.

10 nl/~SCIA_CAL/SCIACALdocuments.php, 2003. 8935, 8956

Noël, S., Bovensmann, H., Wuttke, M. W., Burrows, J. P., Gottwald, M., Krieg, E., Goede, A. P. H., and Muller, C.: Nadir, limb, and occultation measurements with SCIAMACHY, Advances in Space Research, 29, 1819–1824, 2002. 8929

Noël, S., Bovensmann, H., Skupin, J., Wuttke, M. W., Burrows, J. P., Gottwald, M., and Krieg,

15 E.: The SCIAMACHY calibration/monitoring concept and first results, Advances in Space Research, 32, 2123–2128, 2003. 8927, 8934, 8961

Noël, S.: Determination of Correction Factors for SCIAMACHY Radiances and Irradiances (IFE-SCIA-SN-20040618_IrrRadCorrection, issue 5.1), Tech. rep., IfE, http://www.iup.physik. uni-bremen.de/sciamachy/SCIA_CAL/rad_cal.html, 2005. 8956

20 Perron, G.: MIPAS Level 1b Changes & Status, presentation given at the ESA ACVE–2 workshop, http://envisat.esa.int/workshops/acve2/, 2004. 8957

Schrijvers, C.: Relative BRDF (BRDF_rel) keydata based on in-flight measurements (TPD-SCIA-PhE-TN-012), Tech. rep., TNO, 8–20, 2004. 8956

Schutgens, N. A. J., Tilstra, L. G., Stammes, P., and Bréon, F.-M.: On the relationship be-

25 tween Stokes parameters Q and U of atmospheric ultraviolet/visible/near-infrared radiation, J. Geophys. Res. D (Atmospheres), 109(18), D09205, doi:10.1029/2003JD004081, 2004. 8951

Sierk, B.: Study of the imact of ASM diffuser solar spectra on the retrieval of minor trace gases (SCIAMACHY Lv0-1 masterplan workpackage 2.11.1.2.) (IFE-TN-19062003-MB), Tech. rep.,

30 IfE, 2003. 8954

Skupin, J., Noel, S., Wuttke, M. W., Bovensmann, H., Burrows, J. P., Hoogeveen, R., Kleipool, Q., and Lichtenberg, G.: In-flight calibration of the SCIAMACHY solar irradiance spectrum, Advances in Space Research, 32, 2129–2134, 2003. 8955

Title Page

Abstract | Introduction

Conclusions | References

Tables | Figures

◄ | ►

◄ | ►

Back | Close

Full Screen / Esc

Print Version

Interactive Discussion

EGU

Slijkhuis, S.: ENVISAT-1 SCIAMACHY Level 0 to 1c Processing, Algorithm Theoretical Basis Document, issue 2 (ENV-ATB-DLR-SCIA-0041), Tech. rep., DLR, http://atmos.af.op.dlr.de/cgi-bin/h.cgi?page=projdocs, 2000. 8939, 8946, 8948, 8961

Smith, D. L.: AATSR instrument performance verification and optimisation, in: Proceedings of the ENVISAT calibration review (Special publication SP 520), edited by: Sawaya-Lacoste, H., http://envisat.esa.int/calval/proceedings/, 2002. 8957

Tilstra, L. G. and Stammes, P.: Spectral Calibration inconsistency found in the overlap region between channels 2 and 3, Tech. rep., KNMI, http://www.knmi.nl/~tilstra, 2004. 8950

Tilstra, L. G. and Stammes, P.: Alternative polarisation retrieval for SCIAMACHY in the ultraviolet, Atmos. Chem. Phys. Discuss., 5, 1973–1993, 2005, SRef-ID: 1680-7375/acpd/2005-5-1973. 8951, 8952

Tilstra, L. G., de Graaf, M., and Stammes, P.: Verification of SCIAMACHY'S radiometric calibration using GOME colocated Reflectance data, Tech. rep., KNMI, http://www.knmi.nl/~tilstra, 2003. 8955

Tilstra, L. G., van Soest, G., Acarreta, J. R., and Stammes, P.: Verification of the radiometric calibration of SCIAMACHY in the UV for two alternative key data sets, Tech. rep., KNMI, http://www.knmi.nl/~tilstra, 2004. 8974

Tilstra, L. G., Acarreta, J. R., and Stammes, P.: Jumps in the SCIAMACHY Level-1c reflectance spectrum due to failing polarisation correction, in Proceedings ENVISAT/ERS symposium 2004, Salzburg ESA-SP-572, ESA, in print, 2005. 8952

van Soest, G.: Investigation of SCIAMACHY Limb stray light(SRON-EOS-RP-05-006), Tech. rep., SRON, http://www.sron.nl/~SCIA_CAL/SCIACALdocuments.php, 2005. 8944

van Soest, G., Tilstra, L. G., and Stammes, P.: Large-scale validation of SCIAMACHY reflectances in the ultraviolet, Atmos. Chem. Phys. Discuss., 5, 1771–1796, 2005, SRef-ID: 1680-7375/acpd/2005-5-1771. 8955

SCIAMACHY calibration

G. Lichtenberg et al.

EGU

Table 1. Spectral characteristics of the science channels and the PMDs. The detector temperature values are the approximate minimum and maximum value from the year 2004 excluding decontaminations. The PMD wavelength range is defined such that it contains 80% of the signal, the range of the science channels is the total range.

Ch.	Wavelength range [nm]	Resolution [nm]	Temperature Det. [K]	PMD	Wavelength range [nm]
1	212–334	0.24	205.8–207.5	–	–
2	300–412	0.26	205.0–207.0	A	310–365
3	383–628	0.44	224.0–225.0	B	455–515
4	595–812	0.48	223.0–224.3	C	610–690
5	773–1063	0.54	221.4–222.4	D/45	800–900
6	971–1773	1.48	199.0–201.2	E	1500–1635
7	1934–2044	0.22	145.0–149.0	–	–
8	2259–2386	0.26	143.7–147.6	F	2280–2400

EGU
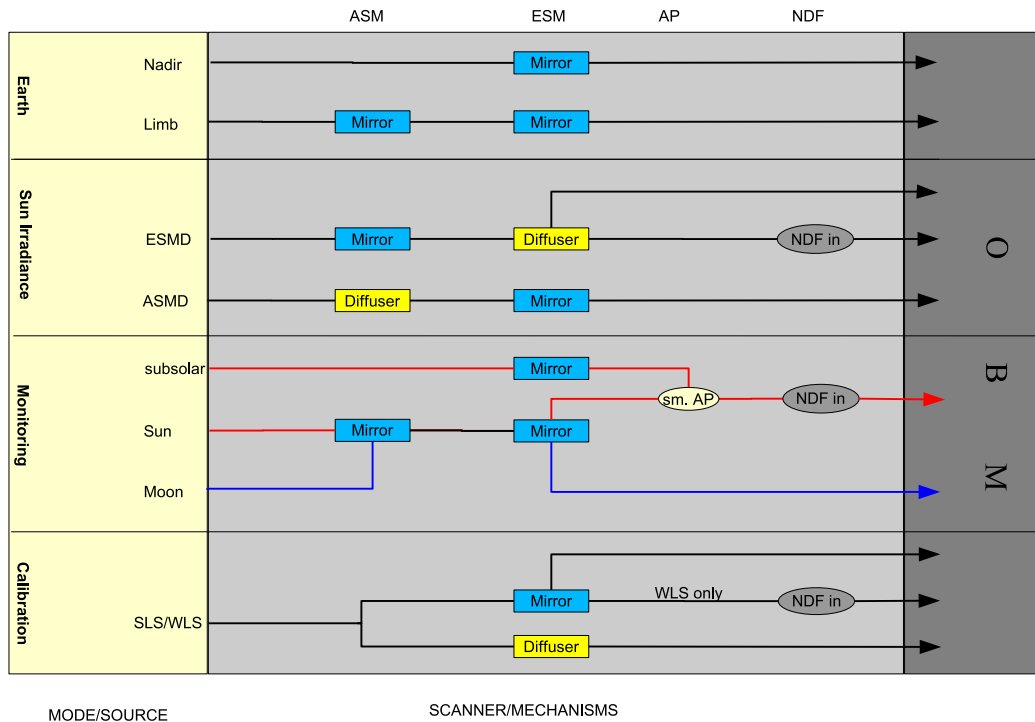
Fig. 1. Simplified optical train of SCIAMACHY for the different observation modes. Only elements not common to all paths are shown. Note that the NDF is only in the light path of channels 3–6. Mirrors are marked blue, diffusers yellow. The optical path in the monitoring mode for the sun is marked red, the path for the moon is marked blue, "sm. AP" denotes the small aperture.
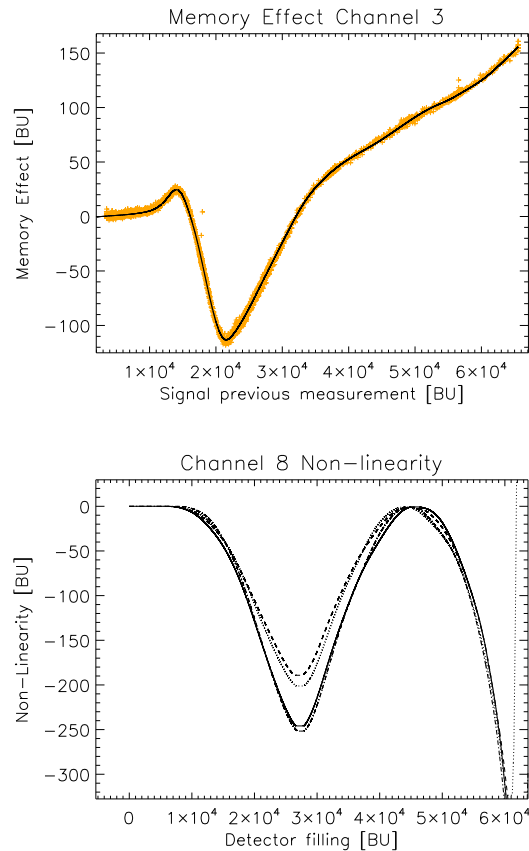
Fig. 2. Top: Memory Effect in channel 3 as a function of the detector signal of the previous readout. Shown is an in-flight measurement from July 2003 (orange crosses) and a spline fit through the data (solid line). Bottom: Non-linearity for channel 8: Low odd pixels (solid), low even pixels (dashed), high odd pixels (dot-dashed) and high even pixels (dotted).

EGU
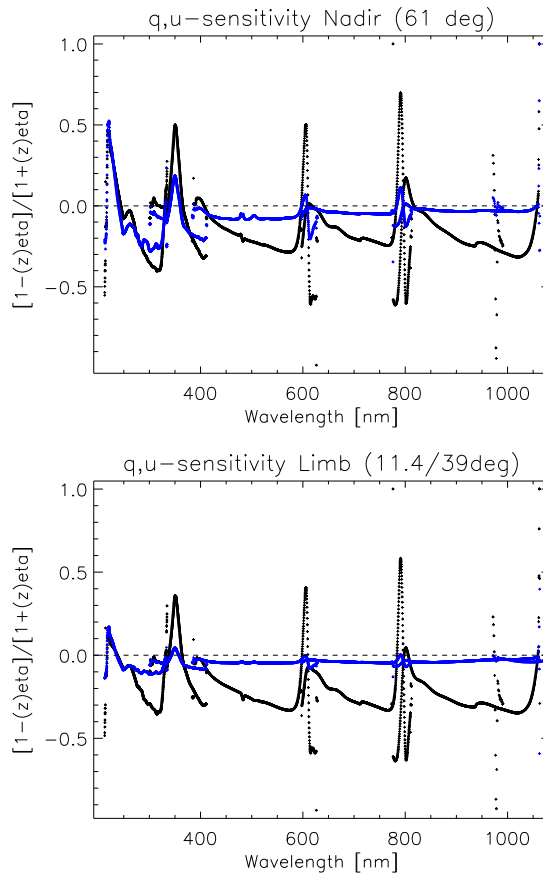
Fig. 3. *q* (black) and *u* (blue) sensitivity from Eq. (11) for Nadir, 61° elevation angle (top) and Limb, 11.4°/39° elevation/azimuth angle (bottom) for channels 1-5. Note that these sensitivities are multiplied with the polarisation fractions to get c_{pol}.

EGU
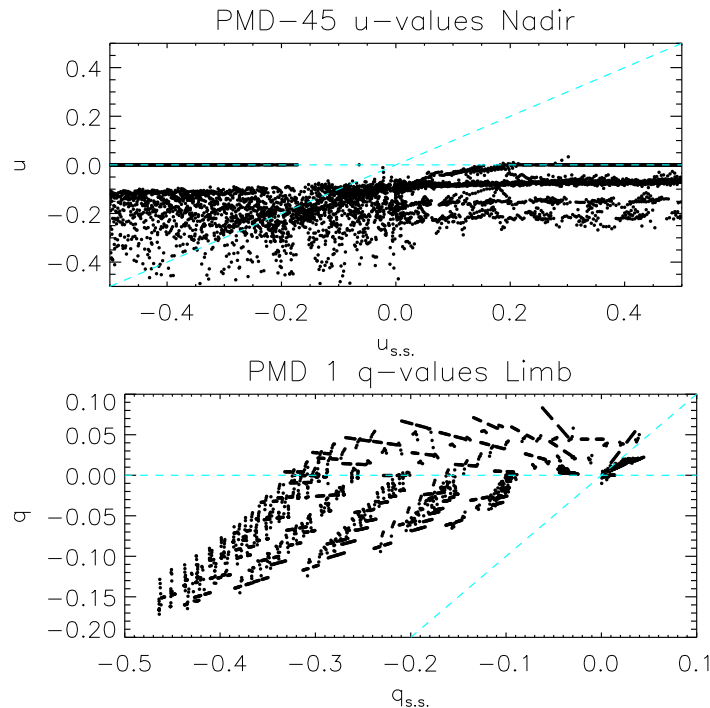
Fig. 4. Top: u values as derived in the processing of PMD 45 and PMD D data for orbit 15975 (21 Marcht 2005). Bottom: q values derived from PMD A (UV, channel 2 wavelength region). Shown is the derived value (y-axis) against the theoretical, single scattering value. The dashed lines mark the unpolarised case and the single scattering case. All derived polarisation fractions outside the dashed lines are not in the physical allowed range. Note that the data were filtered for rainbows and sun glint, so unphysical values are not caused by these effects.

EGU
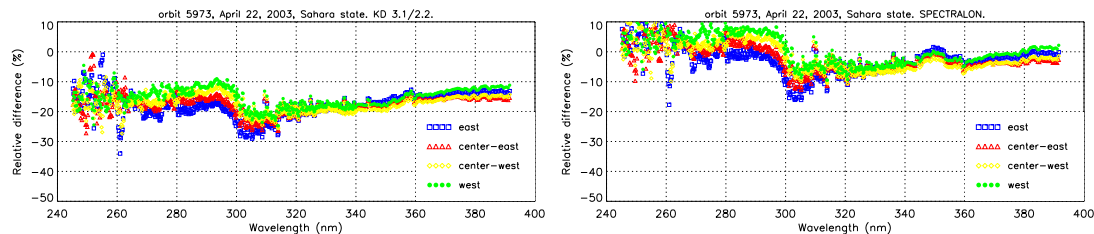
Fig. 5. Comparison of SCIAMACHY calculated reflectance with model calculations, using original calibration data (left) and "spectralon" calibration data (right). It can clearly be seen that the new radiometric calibration improves the overall offset of the reflectance, but also introduces a new spectral feature around 350 nm. Note that the dip around 300nm is probably an artifact caused by insufficient characterisation of the ozone profile in the model (figure taken from Tilstra et al., 2004).

EGU

EGU
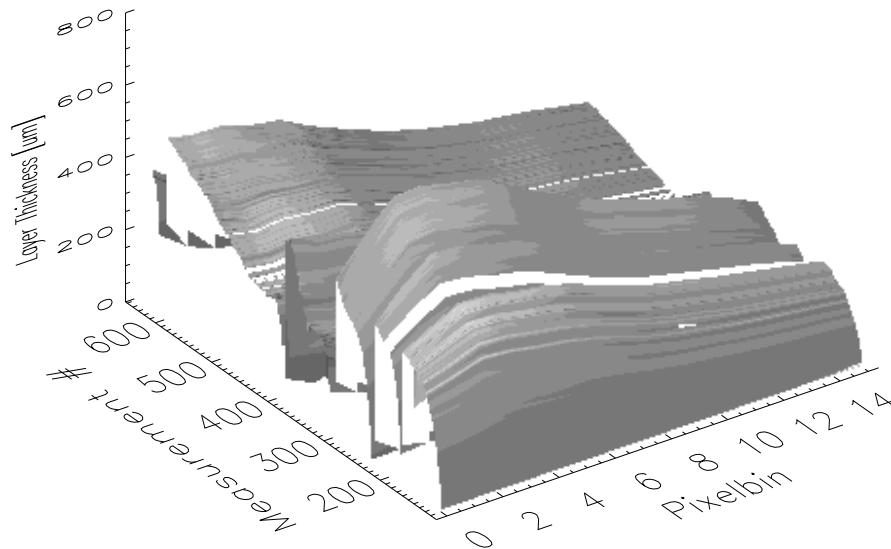
Fig. 6. Ice layer thickness over time and as a function of wavelength for channel 8 derived from solar measurements taken between January 2003 and July 2004. The spectrum was divided into 16 wavelength bands (axis to the right), each band consisting of 64 detector pixels. On the z-axis the thickness of the ice layer is indicated.
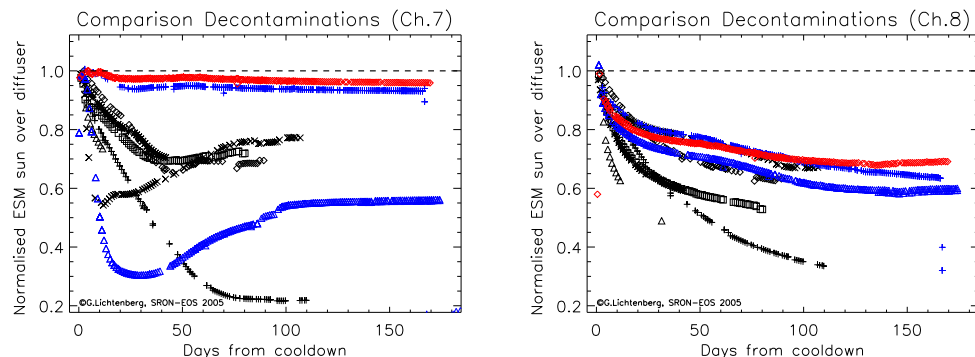
Fig. 7. Comparison of transmission behaviour after decontaminations. Daily updated plots are available at http://www.sron.nl/~SCIA_CAL/SCIACALtransmission.php. Different symbols/colors mark different decontaminations. Shown is the transmission as a function of time since the cool down in days. The development after the decontaminations in December 2003 (crosses) and June 2004 (triangles) are marked blue.The development after the last decontamination in December 2004 is marked in red. All values are normalised to a measurement in January 2003 done shortly after a decontamination removed the ice. Left: channel 7. Right: channel 8.

Title Page

Abstract   Introduction

Conclusions   References

Tables   Figures

◄◄   ►►

◄   ►

Back   Close

Full Screen / Esc

Print Version

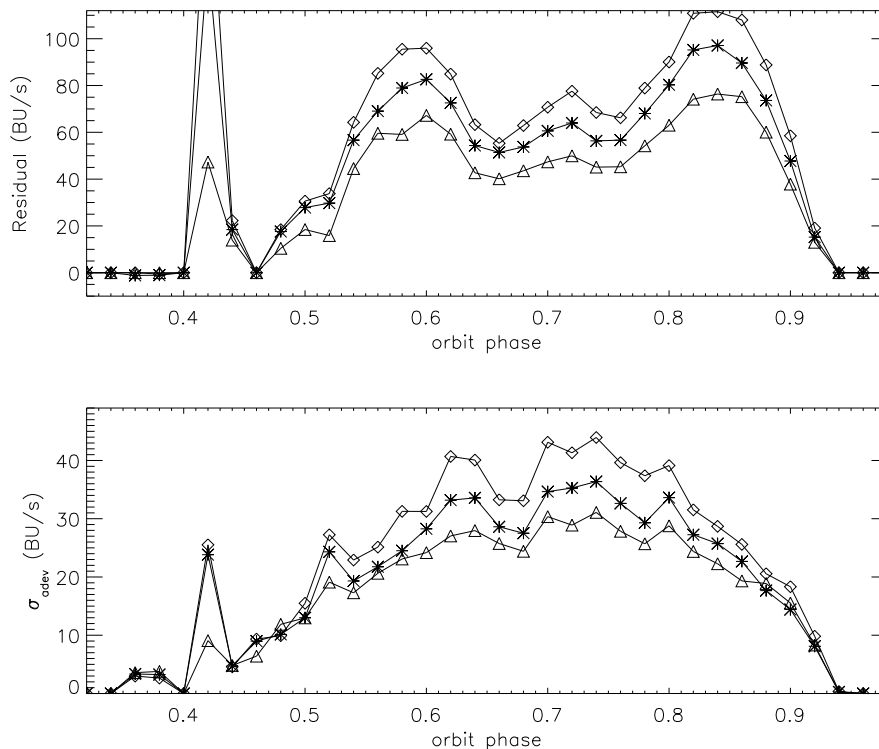Interactive Discussion

[EGU](#)

Fig. 8. Light Leak signal in channel 7 for pixels 103 (triangles), 502 (boxes) and 835 (stars). On the top figure the residual signal after being corrected for nonlinearity, dark measurement and spectral stray light is shown as a function of orbit phase, with phase zero defined as entry of the satellite into eclipse; sunrise occurs around orbit phase 0.4. The high peak seen at that orbit phase is caused by sunlight shining into the limb port and was expected. The bottom figure shows the mean absolute deviation for the same pixels from one month of data.

EGU